International Journal of Thermal Sciences 54 (2012) 142–152

Contents lists available at SciVerse ScienceDirect

International Journal of Thermal Sciences

journal homepage: www.elsevier.com/locate/ijts

Investigation of the gravity effects on the mixed convection heat transfer in a microchannel using lattice Boltzmann method

Arash Karimipour [a], Alireza Hossein Nezhad [a,*], Annunziata D'Orazio [b], Ebrahim Shirani [c]

[a] Department of Mechanical Engineering, University of Sistan and Baluchestan, Zahedan 98135-987, Iran
[b] Dipartimento di Ingegneria Astronautica, Elettrica ed Energetica, Sapienza Università' di Roma, Via Eudossiana 18, Roma 00184, Italy
[c] Department of Mechanical Engineering, Isfahan University of Technology, Isfahan 84156-83111, Iran

ARTICLE INFO

Article history:
Received 2 July 2011
Received in revised form
21 November 2011
Accepted 22 November 2011
Available online 22 December 2011

Keywords:
Gravity
Lattice Boltzmann method
Microchannel
Mixed convection

ABSTRACT

This paper aims to study the gravity effects on the mixed convection heat transfer in a microchannel using lattice Boltzmann method. To include these effects, hydrodynamic boundary condition equations are modified. In this problem, cold fluid enters the microchannel and leaves it after cooling the hot walls. For a wide range of inlet Knudsen number (Kn), computations are performed, and for validation, appropriate comparisons between present and previous available results are made.

As the results, stream lines, longitudinal variations of friction coefficient, Nusselt number, slip velocity and temperature jump, and velocity and temperature profiles in different cross sections are presented. The results show that lattice Boltzmann method can be used to simulate mixed convection in a microchannel, and the effects of buoyancy forces are important for Kn < 0.05, specially for hydrodynamic properties, and thus should be included. For Kn > 0.05, these effects can be ignored. In addition, it is observed that buoyancy forces generate a rotational cell in the microchannel flow, leading to the negative slip velocity at Kn $= 0.005$.

1. Introduction

Nowadays, because of wide applications of MEMS and NEMS (Micro and Nano Electro Mechanical Systems) such as the microsensors, microvalves and micropumps, investigations of flow and heat transfer in microdevices has attracted many researchers. The simulation procedure of the microscopic flows is different from that of macroscopic flows. Microflows are classified according to the Knudsen number defined as $Kn = \lambda/D_H$ in which D_H is the hydraulic diameter (characteristic length) and λ is the molecular mean free path. In microchannel flows, λ may be the same order of magnitude of D_H, thus contradicting the assumption of continuum, which the basic governing equations such as continuity and Navier–Stokes equations are based on. When Kn < 0.001, fluid is continuum and fluid motion is governed by Navier–Stokes equations. But, when Kn > 10, $0.1 <$ Kn < 10 and $0.001 <$ Kn < 0.1, fluid motion is treated as a free molecular, transient and slip flow, respectively [1–6]; These flow regimes may occur in MEMS and should be simulated using particle-based methods, including molecular dynamics (MD) and direct simulation of Monte Carlo (DSMC) methods. The expensive computation cost and complex mathematical equations used in MD and DSMC have recently caused the researchers to seek more-suitable ways like lattice Boltzmann method (LBM) to simulate macro and microflows [7–12].

To simulate the flow and heat transfer of a slip flow, in addition to particle-based methods, the classic Navier–Stokes equations can be used as governing equations, but slip velocity and temperature jump are used as boundary conditions for velocity and temperature on the walls, respectively [13,14].

LBM is a relatively new model to simulate fluid flow. Over a lattice points, the fluid system consists of fictive particles which perform propagation and collision steps. Some of the advantages of LBM over the classic CFD methods are indicated as appropriate dealing with complex boundaries, being able to describe microscopic characteristics and to use parallel algorithms [15–18].

A complementary numerical method to simulate the viscous compressible subsonic flows is LBM BGK; which simulates the flow accurately in different regimes and conditions [19]. Thermal lattice Boltzmann using internal energy distribution function, provides more numerical stability and includes the viscous heat dissipation and pressure work. In this method because of living both of the hydrodynamic and thermal populations on the same lattice, the boundary conditions are simulated easily [20–26].

* Corresponding author. Tel.: +98 541 8052234.
E-mail addresses: arashkarimipour@gmail.com (A. Karimipour), Nezhadd@hamoon.usb.ac.ir (A. Hossein Nezhad), annunziata.dorazio@uniroma1.it (A. D'Orazio), eshirani@ictp.it (E. Shirani).

1290-0729/$ – see front matter © 2011 Elsevier Masson SAS. All rights reserved.
doi:10.1016/j.ijthermalsci.2011.11.015

Nomenclature

$AR = L/H = 30$ aspect ratio
$c = (c_x, c_y)$ microscopic velocity vector
c_s lattice sound speed
C_f friction coefficient
$D_H = 2$ H hydraulic diameter, m
f, g distribution functions for density-momentum and internal energy
$\tilde{f}_i, \tilde{g}_i$ modified discrete distribution functions
$\mathbf{g} = (0, -g)$ gravitational acceleration vector, ms^{-2}
$\mathbf{G} = (0, G)$ buoyancy force per unit mass
$Gr = \beta g \Delta T D_H^3/\upsilon^2$ Grashof number
H, L height and length of the microchannel, m
$Kn = \lambda/D_H$ Knudsen number
$Ma = u_{in}/c_s$ Mach number
Nu Nusselt number
$Pr = \upsilon/\alpha$ Prandtl number
$Re = \rho_{in}\, u_{in}\, D_H/\mu$ Reynolds number
t time, s
T temperature, k
$\mathbf{u} = (u, v)$ macroscopic flow velocity vector, ms^{-1}
$(U,V) = (u/u_{in}, v/u_{in})$ dimensionless flow velocity in x-y direction
$U_s = U_{j\,=\,1,Ny} - U_w$ slip velocity
x, y dimensional Cartesian coordinates, m
(X,Y) = (X/H,Y/H) dimensionless x-y coordinate
Z, Z_i continuous and discrete heat dissipation term

Greek symbols
λ molecular mean free path
$\theta = T/T_{in}$ dimensionless temperature
$\theta_s = \theta_w - \theta_{j\,=\,1,Ny}$ temperature jump
ρ fluid density, kg m^{-3}
τ_f, τ_g relaxation times for density and internal energy

Super- and sub-scripts
e equilibrium
i lattice link number
in inlet flow
out outlet flow
w wall

LBMhas been used to simulate microchannel fluid flow by some researchers. Among them, Lim et al. [27] applied this method to simulate the two-dimensional isothermal pressure driven microchannel flow and concluded that this method is an efficient approach. For simulation of microflows, Niu et al. [28,29] and Shu et al. [30] defined the relaxation time in terms of the Knudsen number and derived the diffuse-scattering boundary condition (DSBC) for the slip velocity. In addition to DSBC, other models have been proposed to simulate slip velocity in microflows [31,32].

Hung and Ru [33] used thermal LBM to study the effects of Knudsen number on the heat transfer and flow behavior in a microchannel. They studied the slip velocity and temperature jump in different Knudsen numbers and presented the temperature distribution in the microchannel flow.

Tian et al. [34] simulated the gaseous flow and heat transfer in microchannels, using thermal LB model with viscous heat dissipation. They proposed a new boundary treatment based on macro variables for the slip velocity and temperature jump, and showed that this model and boundary treatment describe well a thermal microflow with viscous heat effect.

Investigations to find the ways to increase the accuracy of LBM for simulating microflows have led to proposing models such as Multiple-Relaxation time lattice Boltzmann (MRT-LBM) [35] or LBM with D_2Q_{16} scheme [36]. These investigations are still being continued [37–41].

In the previous studies, the effects of gravity in microflows have been ignored, thus decreasing the accuracy of the results. However, in this paper, considering these effects, mixed convection of a flow in a microchannel is investigated numerically using LBM.

2. Problem statement

Flow and mixed convection heat transfer of air in a two-dimensional microchannel, as shown in Fig. 1, are studied numerically, using double population lattice Boltzmann method and employing BGK and thermal energy distribution models for the cases Kn = 0.005, 0.01, 0.05 and 0.1. Reynolds number at the inlet is usually small in the microchannel, so it is assumed that $Re = \rho_{in}\, u_{in}\, D_H/\mu = 1$ and $Pr = \upsilon/\alpha = 0.7$. In this method, hydrodynamic and thermal parameters of fluid flow are estimated using density-momentum distribution function, f, and internal energy density distribution function, g, respectively.

Wall temperature is assumed twice as much as the inlet fluid temperature, $T_w = 2\ T_{in,}$ and the ratio of microchannel length, L, to its width, H, is assumed as 30; thus after entrance length, fully developed condition for velocity and temperature is being satisfied.

Two cases are studied. In the first case (A) the effects of gravity are ignored, and in the second case (B), $Gr = \beta g \Delta T D_H^3/\upsilon^2$, involving gravity, is employed to study these effects. β is the volumetric expansion coefficient, $\Delta T = T_w - T_{in}$ and υ is the kinematic viscosity. The results are obtained for different Kn's and compared with one another.

Gravity acceleration causes vertical component of velocity to be affected by buoyancy force. To include this effect, the hydrodynamic boundary condition equations are modified. For a wide range of inlet Knudsen number, computations are performed, and for validation, appropriate comparisons between present and previous available results are made.

3. Mathematical formulation

3.1. Lattice Boltzmann method

The Boltzmann equation of single-particle distribution function is written as follows [20]:

$$\partial_t f + (c \cdot \nabla) f = \Omega(f) \tag{1}$$

where Ω is the collision term. Eq. (1) and thermal energy distribution model are used to simulate flow and heat transfer, respectively. In this method internal energy distribution function is defined as:

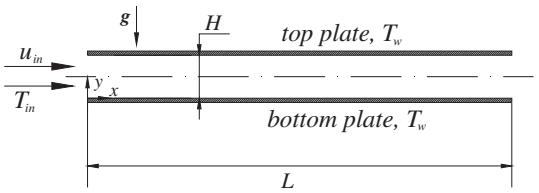

Fig. 1. Microchannel configuration.

$$g = 0.5(\boldsymbol{c}-\boldsymbol{u})^2 f \tag{2}$$

Lattice Boltzmann equation based on internal energy distribution function is defined as:

$$\partial_t g + (\boldsymbol{c}\cdot\nabla)g = \Omega(g) \tag{3}$$

Collision term of Boltzmann equation in BGK model is written as follow [19,20]:

$$\Omega(f) = -\frac{f-f^e}{\tau_f} \tag{4}$$

$$\Omega(g) = -\frac{g-g^e}{\tau_g} - fZ = 0.5(\boldsymbol{c}-\boldsymbol{u})^2\Omega(f) - fZ \tag{5}$$

where fZ is the heat dissipation term and can be defined as:

$$fZ = f(\boldsymbol{c}-\boldsymbol{u})\cdot[\partial_t \boldsymbol{u} + (\boldsymbol{c}\cdot\nabla)\boldsymbol{u}] \tag{6}$$

τ_f and τ_g are the relaxation times. To solve the difficulty of the implicitness of the scheme, two new distribution functions $\tilde{f}_i$ and $\tilde{g}_i$ are defined as follows:

$$\tilde{f}_i = f_i + \frac{dt}{2\tau_f}(f_i - f_i^e) \tag{7}$$

$$\tilde{g}_i = g_i + \frac{dt}{2\tau_g}(g_i - g_i^e) + \frac{dt}{2} f_i Z_i \tag{8}$$

where f_i^e and g_i^e are discretized Maxwell–Boltzmann equilibrium distribution functions for density and internal energy. The subscript i denotes the number of the link in the D_2Q_9 lattice shown in Fig. 2 [42] and used in the present work, and Z_i is defined as:

$$Z_i = (\boldsymbol{c}_i - \boldsymbol{u})\cdot D_i\boldsymbol{u} \text{ and } D_i = \partial_t + \boldsymbol{c}_i\cdot\nabla \tag{9}$$

$$\begin{aligned}
\boldsymbol{c}_i &= \left(\cos\frac{i-1}{2}\pi, \sin\frac{i-1}{2}\pi\right)\boldsymbol{c}, i = 1,2,3,4\\
\boldsymbol{c}_i &= \sqrt{2}\left(\cos\left[\frac{(i-5)}{2}\pi + \frac{\pi}{4}\right], \sin\left[\frac{(i-5)}{2}\pi + \frac{\pi}{4}\right]\right)\boldsymbol{c},\ i = 5,6,7,8\\
\boldsymbol{c}_0 &= (0,0)
\end{aligned} \tag{10}$$

$\mathbf{c}_i$ is the discrete particle lattice velocity. Using equilibrium distribution functions f^e and g^e the collision and propagation stages are stated as:

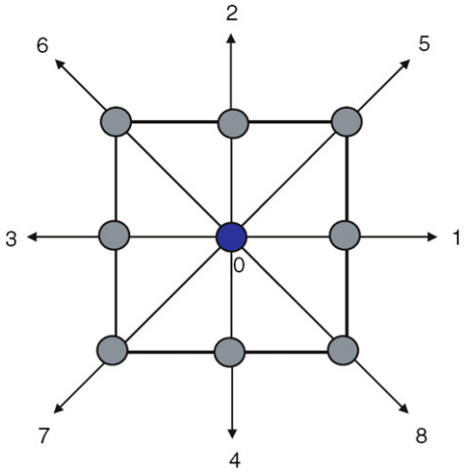

Fig. 2. D_2Q_9 lattice.

$$\tilde{f}_i(\boldsymbol{x}+\boldsymbol{c}_i dt, t+dt) - \tilde{f}_i(\boldsymbol{x},t) = -\frac{dt}{\tau_f + 0.5dt}\left[\tilde{f}_i - f_i^e\right] \tag{11}$$

$$\begin{aligned}
\tilde{g}_i(\boldsymbol{x}+\boldsymbol{c}_i dt, t+dt) - \tilde{g}_i(\boldsymbol{x},t) &= -\frac{dt}{\tau_g + 0.5dt}\left[\tilde{g}_i - g_i^e\right]\\
&\quad - \frac{\tau_g dt}{\tau_g + 0.5dt} f_i Z_i
\end{aligned} \tag{12}$$

$$f_i^e = \omega_i\rho\left[1 + \frac{3\boldsymbol{c}_i\cdot\boldsymbol{u}}{c^2} + \frac{9(\boldsymbol{c}_i\cdot\boldsymbol{u})^2}{2c^4} - \frac{3(u^2+v^2)}{2c^2}\right] \tag{13}$$

$$\begin{aligned}
g_0^e &= -\omega_0\left[\frac{3\rho e}{2}\frac{u^2+v^2}{c^2}\right]\\
g_{1,2,3,4}^e &= \omega_1\rho e\left[1.5 + 1.5\frac{\boldsymbol{c}_i\cdot\boldsymbol{u}}{c^2} + 4.5\frac{(\boldsymbol{c}_i\cdot\boldsymbol{u})^2}{c^4} - 1.5\frac{u^2+v^2}{c^2}\right]\\
g_{5,6,7,8}^e &= \omega_2\rho e\left[3 + 6\frac{\boldsymbol{c}_i\cdot\boldsymbol{u}}{c^2} + 4.5\frac{(\boldsymbol{c}_i\cdot\boldsymbol{u})^2}{c^4} - 1.5\frac{u^2+v^2}{c^2}\right]
\end{aligned} \tag{14}$$

where in a two-dimensional lattice, $\boldsymbol{c}^2 = 3\mathrm{RT} = 1$, $\rho e = \rho\,\mathrm{RT}$ and the weights of the functions are as $\omega_0 = 4/9$ and $\omega_i = 1/9$, $i = 1, 2, 3, 4$ and $\omega_i = 1/36$, $i = 5, 6, 7, 8$. Finally the hydrodynamic and thermal variables are calculated as follows [22,23]:

$$\begin{aligned}
\rho &= \sum_i \tilde{f}_i\\
\rho\boldsymbol{u} &= \sum_i \boldsymbol{c}_i\tilde{f}_i\\
\rho e &= \sum_i \tilde{g}_i - \frac{dt}{2}\sum_i f_i Z_i
\end{aligned} \tag{15}$$

The Knudsen number according to the kinetic theory can be stated as:

$$Kn = \sqrt{\frac{\pi k}{2}}\frac{Ma}{\mathrm{Re}} \tag{16}$$

where k, heat capacity ratio of gas, is 7/5 for diatomic ideal gas. Using definition of Re, $Ma = u_{in}/c_s$, $\tau = \mu/P$, $P = \rho c_s^2$ and lattice sound speed $c_s = 1/3^{0.5}$, we can write [28–30]:

$$\tau_f = \sqrt{\frac{6}{\pi k}} D_H \cdot Kn \tag{17}$$

$$\tau_g = \frac{\tau_f}{\mathrm{Pr}} \tag{18}$$

3.2. Boundary conditions

Non-equilibrium bounce back model, normal to the boundary is used for the inlet and outlet hydrodynamic boundary conditions [43,44]:

$$\begin{aligned}
\tilde{f}_1 &= \tilde{f}_3 + \frac{2}{3}\rho_{in}u_{in}\\
\tilde{f}_5 &= \tilde{f}_7 + \frac{1}{2}\left(\tilde{f}_4 - \tilde{f}_2\right) + \frac{1}{6}\rho_{in}u_{in}\\
\tilde{f}_8 &= \tilde{f}_6 - \frac{1}{2}\left(\tilde{f}_4 - \tilde{f}_2\right) + \frac{1}{6}\rho_{in}u_{in}
\end{aligned} \tag{19}$$

Table 1
Grid dependence study for the case A at $Re = 1$, $Pr = 0.7$ and Kn = 0.01.

	1050 × 35	1200 × 40	1350 × 45
Nu	7.54	7.60	7.62
C_fRe	22.29	22.36	22.39

$$\begin{aligned}\tilde{f}_3 &= \tilde{f}_1 - \frac{2}{3}\rho_{out}u_{out}\\ \tilde{f}_7 &= \tilde{f}_5 - \frac{1}{2}\left(\tilde{f}_4 - \tilde{f}_2\right) - \frac{1}{6}\rho_{out}u_{out} - \frac{1}{2}\rho_{out}v_{out}\\ \tilde{f}_6 &= \tilde{f}_8 + \frac{1}{2}(\tilde{f}_4 - \tilde{f}_2) - \frac{1}{6}\rho_{out}u_{out} + \frac{1}{2}\rho_{out}v_{out}\end{aligned} \tag{20}$$

Using the same method, at the inlet of the microchannel, having known temperature profile, the unknown distribution functions are calculated using relations stated in Eq. (21), and at the outlet, thermal boundary condition is defined as the relations of Eq. (22) [23]:

$$\begin{aligned}\tilde{g}_5 &= \frac{6\rho e + 3dt\sum_i f_i Z_i - 6\left(\tilde{g}_0 + \tilde{g}_2 + \tilde{g}_3 + \tilde{g}_4 + \tilde{g}_6 + \tilde{g}_7\right)}{2 + 3u_{in} + 3u_{in}^2}\\ &\quad\times\left[3.0 + 6u_{in} + 3.0u_{in}^2\right]\frac{1}{36}\\ \tilde{g}_1 &= \frac{6\rho e + 3dt\sum_i f_i Z_i - 6\left(\tilde{g}_0 + \tilde{g}_2 + \tilde{g}_3 + \tilde{g}_4 + \tilde{g}_6 + \tilde{g}_7\right)}{2 + 3u_{in} + 3u_{in}^2}\\ &\quad\times\left[1.5 + 1.5u_{in} + 3.0u_{in}^2\right]\frac{1}{9}\\ \tilde{g}_8 &= \frac{6\rho e + 3dt\sum_i f_i Z_i - 6\left(\tilde{g}_0 + \tilde{g}_2 + \tilde{g}_3 + \tilde{g}_4 + \tilde{g}_6 + \tilde{g}_7\right)}{2 + 3u_{in} + 3u_{in}^2}\\ &\quad\times\left[3.0 + 6u_{in} + 3.0u_{in}^2\right]\frac{1}{36}\end{aligned} \tag{21}$$

$$\begin{aligned}\tilde{g}_6 &= \frac{6\left(\tilde{g}_1 + \tilde{g}_5 + \tilde{g}_8\right) - 3dt\sum_i\left(\frac{c_{ix}}{c}\right)Z_i f_i - 6\rho e u_{out}}{2 - 3u_{out} + 3u_{out}^2}\\ &\quad\times\left[3.0 - 6.0u_{out} + 6.0v_{out} + 3.0u_{out}^2 + 3.0v_{out}^2 - 9.0u_{out}v_{out}\right]\frac{1}{36}\\ \tilde{g}_3 &= \frac{6\left(\tilde{g}_1 + \tilde{g}_5 + \tilde{g}_8\right) - 3dt\sum_i\left(\frac{c_{ix}}{c}\right)Z_i f_i - 6\rho e u_{out}}{2 - 3u_{out} + 3u_{out}^2}\\ &\quad\times\left[1.5 - 1.5u_{out} + 3.0u_{out}^2 - 1.50v_{out}^2\right]\frac{1}{9}\\ \tilde{g}_7 &= \frac{6\left(\tilde{g}_1 + \tilde{g}_5 + \tilde{g}_8\right) - 3dt\sum_i\left(\frac{c_{ix}}{c}\right)Z_i f_i - 6\rho e u_{out}}{2 - 3u_{out} + 3u_{out}^2}\\ &\quad\times\left[3.0 - 6.0u_{out} - 6.0v_{out} + 3.0u_{out}^2 + 3.0v_{out}^2 + 9.0u_{out}v_{out}\right]\frac{1}{36}\end{aligned} \tag{22}$$

Using specular reflective bounce back and diffuse-scattering boundary condition (DSBC), the slip velocity and temperature jump are calculated on the walls [37,28].

The specular bounce back is the combination of bounce back and specular boundary condition. In the DSBC, the particles colliding with the solid wall forget their information and they are reflected consistently with the Maxwellian distribution function.

To determine slip velocity on the microchannel bottom wall, the unknown distribution functions are written as:

$$\tilde{f}_2 = \tilde{f}_4 \tag{23-1}$$

$$\tilde{f}_{5,6} = r\tilde{f}_{7,8} + (1 - r)\tilde{f}_{8,7} \tag{23-2}$$

To obtain more accurate results, the value of accommodation coefficient, r, is chosen appropriately in the range of $r < 1$ [15,45,46].

The slip velocity on the top wall is calculated similarly. The temperature jump on the bottom wall of the microchannel is calculated using Eq. (24).

$$\tilde{g}_{2,5,6} = \frac{3}{\rho_w e}g^e_{2,5,6}(\rho_w, \boldsymbol{u}_w, e_w)\left(\tilde{g}_4 + \tilde{g}_7 + \tilde{g}_8\right) \tag{24}$$

where ρ_w and $\boldsymbol{u}_w$ are density and velocity on the wall, respectively. Temperature jump on the top wall is calculated similarly.

3.3. Effects of gravity

In the previous equations, forced heat transfer has been discussed and the effects of gravity on the flow and heat transfer have been ignored. However, in this paper, the effects of mixed convection in a microchannel are investigated. To incorporate the effects of free convection into the LBM equations, Boussinesq approximation is used. In this approximation buoyancy forces is defined as $G = \beta g(T - \overline{T})$ in which $\overline{T}$ is average temperature.

According to the definitions of *Gr*, Kn, *Re* and *Ma* and using Eq. (16), the dependence of the Kn on *Gr* is observed. So, in this work for air, Kn = 0.005 and $Gr = 1328$ are used. For the other cases, having known Kn, the corresponding value of *Gr* is calculated and used in the solution of the problem. For all the cases, physical properties of air in the real conditions are used, so that Boussinesq approximation conditions including the permissible limit of temperature difference is satisfied, and the problem is solved with physical assumptions.

Considering the effect of external force, F, the Boltzmann equation is written as the following [20].

$$\partial_t f + (\boldsymbol{c}\cdot\nabla)f = -\frac{f - f^e}{\tau_f} + F \tag{25}$$

where buoyancy force can be state as $F = (\boldsymbol{G}\cdot(\boldsymbol{c} - \boldsymbol{u})/RT)f^e$.

In the following, a second-order strategy is employed to integrate the Boltzmann Eq. (25).

Table 2
Comparison of natural convection cavity flow results obtained from the present work with those of Davis [47] at $Pr = 0.7$ and different Ra's: v_{max}/V^* is maximum vertical velocity at $y/H = 0.5$, u_{max}/V^* is maximum horizontal velocity at $x/L = 0.5$, and their locations are stated in parentheses.

Ra	U_{max} (y/H)			V_{max} (x/L)			Nu_m		
	Present	Davis [47]	Error%	Present	Davis [47]	Error%	Present	Davis [47]	Error%
10^4	15.951 (0.817)	16.178 (0.823)	−1.403 (−0.729)	19.338 (0.123)	19.617 (0.119)	−1.422 (3.361)	2.210	2.243	−1.471
10^5	34.239 (0.851)	34.730 (0.855)	−1.414 (−0.468)	67.501 (0.067)	68.590 (0.066)	−1.588 (1.515)	4.456	4.519	−1.394
10^6	64.088 (0.846)	64.630 (0.850)	−0.839 (−0.470)	214.35 (0.033)	219.360 (0.0379)	−2.284 (−12.929)	8.756	8.800	−0.500

$$f(\boldsymbol{x}+\boldsymbol{c}dt,\boldsymbol{c},t+dt)\ -f(\boldsymbol{x},\boldsymbol{c},t)\ =\ -\frac{dt}{2\tau_f}[f(\boldsymbol{x}+\boldsymbol{c}dt,\boldsymbol{c},t+dt) -f^e(\boldsymbol{x}+\boldsymbol{c}dt,\boldsymbol{c},t+dt)] -\frac{dt}{2\tau_f}[f(\boldsymbol{x},\boldsymbol{c},t)-f^e(\boldsymbol{x},\boldsymbol{c},t)]\ +\frac{dt}{2}F(\boldsymbol{x}+cdt,\boldsymbol{c},t+dt)\ +\frac{dt}{2}F(\boldsymbol{x},\boldsymbol{c},t) \tag{26}$$

Using $\tilde{f}_i = f_i + 0.5dt/\tau_f(f_i - f_i^e) - 0.5dtF$, the Eq. (26) is written as follows.

$$\tilde{f}(\boldsymbol{x}+\boldsymbol{c}dt,\boldsymbol{c},t+dt)\ -\tilde{f}(\boldsymbol{x},\boldsymbol{c},t)\ =\ -\frac{dt}{\tau_f+0.5dt}\left[\tilde{f}(\boldsymbol{x},\boldsymbol{c},t) -f^e(\boldsymbol{x},\boldsymbol{c},t)\right]\ +\frac{\tau_f F dt}{\tau_f+0.5dt} \tag{27}$$

Discretization of the above equation leads to

$$\tilde{f}_i(\boldsymbol{x}+\boldsymbol{c}_i\mathrm{d}t,t+\mathrm{d}t)\ -\tilde{f}_i(\boldsymbol{x},t)\ =\ -\frac{\mathrm{d}t}{\tau_f+0.5\mathrm{d}t}\left[\tilde{f}_i-f_i^e\right] +\left(\frac{\mathrm{d}t\tau_f}{\tau_f+0.5\mathrm{d}t}\frac{3G(c_{iy}-v)}{c^2}f_i^e\right) \tag{28}$$

$$f_i\ =\ \frac{\tau_f\tilde{f}_i+0.5\mathrm{d}tf_i^e}{\tau_f+0.5\mathrm{d}t}+\left(\frac{0.5\mathrm{d}t\tau_f}{\tau_f+0.5\mathrm{d}t}\frac{3G(c_{iy}-v)}{c^2}f_i^e\right) \tag{29}$$

Now the macroscopic variables can be calculated using the following relations [20].

$$\rho\ =\ \sum_i\tilde{f}_i \tag{30-1}$$

$$u\ =\ (1/\rho)\sum_i\tilde{f}_ic_{ix} \tag{30-2}$$

$$v\ =\ (1/\rho)\sum_i\tilde{f}_ic_{iy}+\frac{\mathrm{d}t}{2}G \tag{30-3}$$

Inlet hydrodynamic boundary conditions are affected by gravity, and by using Eqs. (30-1), (30-2) and (30-3), the following relations are obtained.

$$\tilde{f}_1+\tilde{f}_5+\tilde{f}_8\ =\ \rho_{in}-\left(\tilde{f}_0+\tilde{f}_2+\tilde{f}_3+\tilde{f}_4+\tilde{f}_6+\tilde{f}_7\right) \tag{31-1}$$

$$\tilde{f}_1+\tilde{f}_5+\tilde{f}_8\ =\ \rho_{in}u_{in}+\left(\tilde{f}_3+\tilde{f}_6+\tilde{f}_7\right) \tag{31-2}$$

$$\tilde{f}_5-\tilde{f}_8\ =\ \rho_{in}v_{in}+\left(-\tilde{f}_2+\tilde{f}_4-\tilde{f}_6+\tilde{f}_7\right)\ -\frac{dt}{2}\rho_{in}G \tag{31-3}$$

From these relations, ρ_{in}, by a simple mathematical procedure, is obtained as

$$\rho_{in}\ =\ \frac{\tilde{f}_0+\tilde{f}_2+\tilde{f}_4+2\left(\tilde{f}_3+\tilde{f}_6+\tilde{f}_7\right)}{1-u_{in}} \tag{32}$$

Non-equilibrium bounce back boundary condition normal to the boundary is calculated as

$$\tilde{f}_1-\tilde{f}_1^e\ =\ \tilde{f}_3-\tilde{f}_3^e\Rightarrow\tilde{f}_1\ =\ \tilde{f}_3-\tilde{f}_3^e+\tilde{f}_1^e \tag{33}$$

Using Eq. (13)

$$\tilde{f}_1\ =\ \tilde{f}_3+\frac{2}{3}\rho_{in}u_{in} \tag{34}$$

Using Eqs. (31-2), (31-3) and (34),

$$\begin{aligned}\tilde{f}_8\ &=\ \tilde{f}_6-\frac{\tilde{f}_4-\tilde{f}_2}{2}+\frac{1}{6}\rho_{in}u_w-\frac{1}{2}\rho_{in}v_{in}+\frac{\mathrm{d}t}{4}\rho_{in}G\\ \tilde{f}_5\ &=\ \tilde{f}_7+\frac{\tilde{f}_4-\tilde{f}_2}{2}+\frac{1}{6}\rho_{in}u_{in}+\frac{1}{2}\rho_{in}v_{in}-\frac{\mathrm{d}t}{4}\rho_{in}G\end{aligned} \tag{35}$$

Similarly, outlet hydrodynamic boundary conditions are written as follows.

$$\begin{aligned}\tilde{f}_3\ &=\ \tilde{f}_1-\frac{2}{3}\rho_{out}u_{out}\\ \tilde{f}_7\ &=\ \tilde{f}_5-\frac{1}{2}\left(\tilde{f}_4-\tilde{f}_2\right)\ -\frac{1}{6}\rho_{out}u_{out}-\frac{1}{2}\rho_{out}v_{out}+\frac{1}{4}\mathrm{d}t\rho_{out}G\\ \tilde{f}_6\ &=\ \tilde{f}_8+\frac{1}{2}\left(\tilde{f}_4-\tilde{f}_2\right)\ -\frac{1}{6}\rho_{out}u_{out}+\frac{1}{2}\rho_{out}v_{out}-\frac{1}{4}\mathrm{d}t\rho_{out}G\end{aligned} \tag{36}$$

In order to include the buoyancy force effects, the slip velocity, Eq. (23), must satisfy the constraint (30-3). As an example, for the bottom wall, the unknown distribution functions are $\tilde{f}_2,\tilde{f}_5,\tilde{f}_6$ and the mentioned constraint is written as

$$\tilde{f}_2+\tilde{f}_5+\tilde{f}_6\ =\ \rho_wv_w+\left(\tilde{f}_4+\tilde{f}_7+\tilde{f}_8\right)\ -\frac{\mathrm{d}t}{2}\rho_wG \tag{37}$$

To satisfy the above equation and include buoyancy force effect, the slip velocity is written as follows.

$$\begin{aligned}\tilde{f}_2\ &=\ \tilde{f}_4-\frac{1}{2}\mathrm{d}t\rho G\\ \tilde{f}_5\ &=\ r\tilde{f}_7+\left(1-r\right)\tilde{f}_8\\ \tilde{f}_6\ &=\ r\tilde{f}_8+\left(1-r\right)\tilde{f}_7\end{aligned} \tag{38}$$

Nu and C_f along the microchannel wall are calculated as

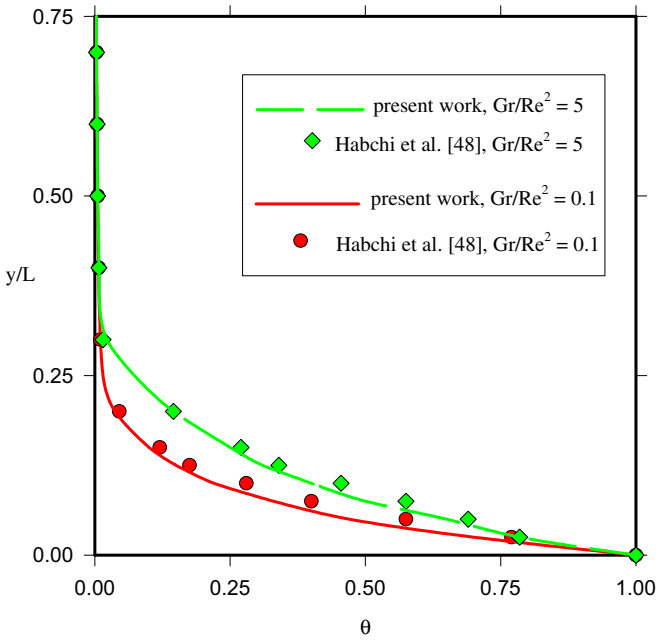

Fig. 3. Comparison of the variations of θ at the channel cross section x/L = 0.77 obtained from the present work with those of Habchi et al. [48] for the case Pr = 0.7 and Ra = 10^5.

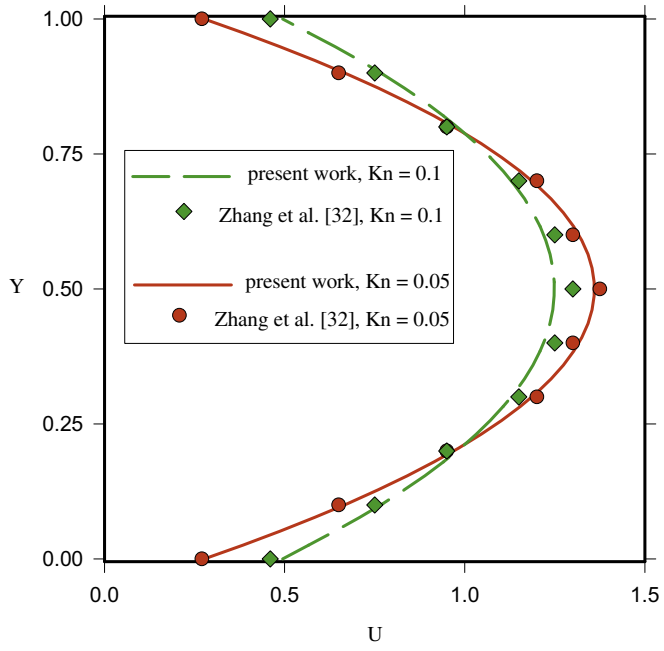

Fig. 4. Validation of fully developed dimensionless velocity profile, U, with those of Zhang et al. [32] for the cases Kn = 0.05, 0.1.

$$Nu = \frac{D_H(\partial T/\partial y)_w}{T_w - T_{balk}} \tag{39}$$

$$C_f = \frac{2\mu(\partial u/\partial y)_w}{\rho u_{balk}^2} \tag{40}$$

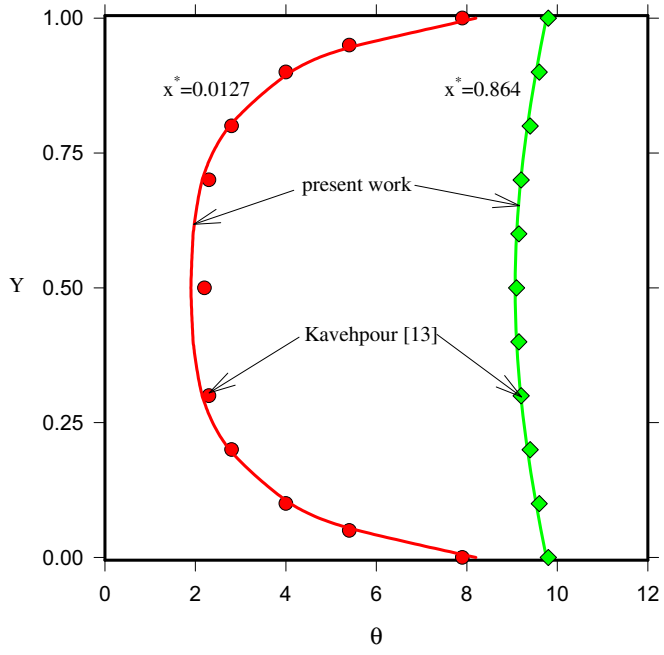

Fig. 5. Validation of θ in different cross sections of a microchannel for $Re = 0.01$, $T_{wall} = 10$, $T_{inlet} = 1$, $Pr = 0.7$ and $Kn_{in} = 0.01$ with those of Kavehpour et al. [13].

Table 3
Comparison of *Nu* and C_fRe defined on the walls at the outlet of michrochannel for the case A at $Re = 0.01$ and two different Kn's.

	C_fRe [13]	C_fRe [28]	C_fRe [present work]	Nu [13]	Nu [28]	*Nu* [present work]
Kn = 0.015	21.80	21.49	21.10	7.38	7.42	7.23
Kn = 0.046	18.45	18.20	18.01	6.58	6.60	6.63

4. Grid independency and numerical validation

A computer code in FORTRAN language was developed to investigate flow and mixed convection in a two-dimensional microchannel. Having studied grid independency shown in Table 1, a lattice with 1200 × 40 nodes is selected as an appropriate one for the next studies.

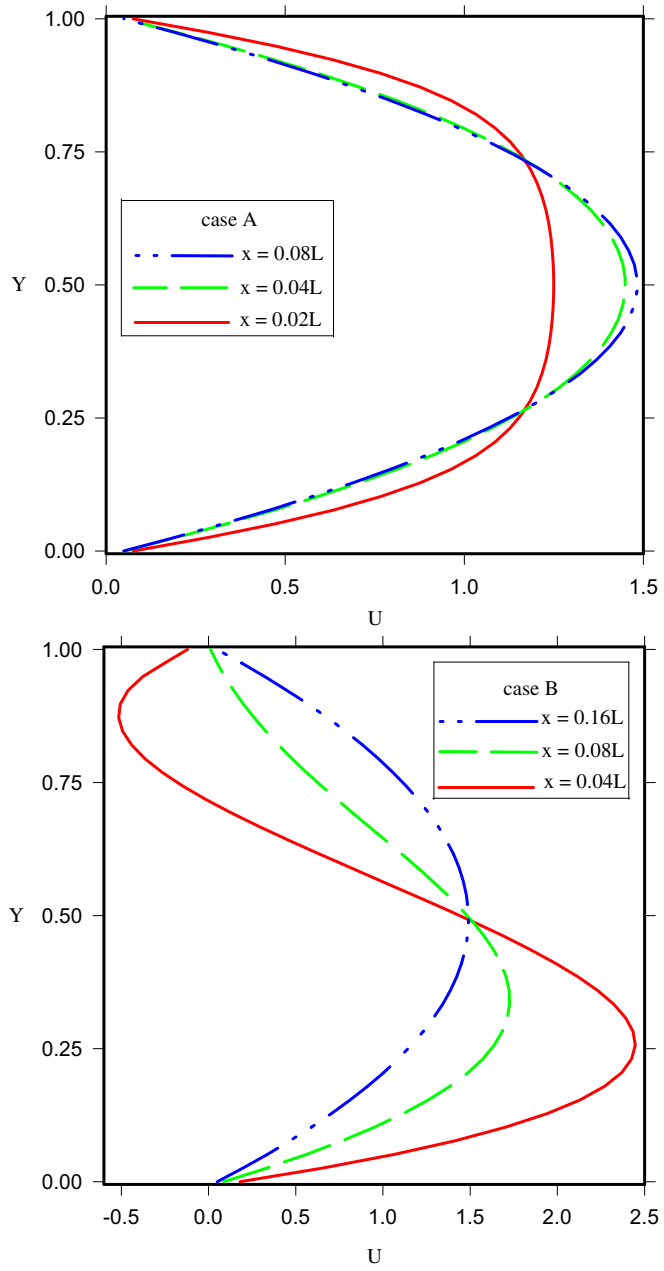

Fig. 6. Profiles of horizontal component of velocity, U, in different cross sections at Kn = 0.005 for the cases A and B.

Because the mixed convection in a microchannel, according to the author's knowledge, is a novel problem, no data are found to validate the present problem. Instead, the validation is performed in two parts. In part one, the computer code based on LBM, is used to simulate natural convection in a cavity and mixed convection in a channel, and then the results are compared with the previous available ones. In the second part, fluid flow and forced heat transfer in a microchannel is validated.

For the first validation of part 1, the benchmarck numerical solution in a square cavity with height of H and horizontal adiabatic walls is considered. The vertical walls are at different temperatures. For different Rayleigh numbers ($Ra = \beta g \Delta T H^3/\upsilon\alpha$) at $Pr = 0.7$ the natural convention is simulated utilizing LBM and the results are compared with those of Davis [47] with classic Navier Stokes method in Table 2. In this table Nu_m is the average Nusselt number, u_{max}/V^* at $x/L = 0.5$ and v_{max}/V^* at $y/H = 0.5$ are maximum horizontal and vertical velocities, respectively; $V^* = \upsilon/PrH$ is a diffusion velocity. The comparison shows good agreement between present results with those of Ref. [47].

For the second validation of this part, mixed convection in a vertical channel is selected. The inlet cold temperature is assumed as T_0, left wall is assumed adiabatic, and the hot right wall ($y = 0$) temperature is assumed as T_h while a hot block is attached to. Temperature profile $\theta=(T-T_0)/(T_h-T_0)$ for $Gr/Re^2 = 0.1, 5$ and $Ra = 10^5$ and $Pr = 0.7$, in horizontal cross section of channel at $x/L = 0.77$ are compared in Fig. 3 with those of Habchi et al. [48].

For the validation of part 2, the fully developed dimensionless velocity profiles, $U = u/u_{in}$, for $Kn = 0.05, 0.1$ at the cross sections of the microchannel are compared with those of Zhang et al. [32] in Fig. 4. Moreover, dimensionless temperature profiles, $\theta = T/T_{in}$, at cross sections $x^* = 0.864, 0.0127$ along the microchannel are compared with those of Kavehpour et al. [13] in Fig. 5 for $Re = 0.01$, $T_{wall} = 10$, $T_{inlet} = 1$, $Pr = 0.7$ and $Kn_{in} = 0.01$. In both of these figures, good agreements are observed. In another validation, a microchannel with geometry, flow and thermal boundary conditions similar to the one studied in Refs. [13,28] is selected, in which cold flow enters with $Re = 0.01$, and leaves after cooling the hot walls. Table 3 shows good agreement between the results of present work and the corresponding ones of those references.

5. Results and discussions

Using lattice Boltzmann BGK method, the flow and mixed convection in a two-dimensional microchannel is studied numerically. As stated before, in the following, studies are performed for the cases A and B. Fig. 6 (for $Kn = 0.005$) and Fig. 7 (for $Kn = 0.01$) show profiles of horizontal component of velocity, $U = u/u_{in}$, in different cross sections. Fig. 6 shows that in the case A, flow after traveling a short distance from the inlet, called entrance length, reaches to the fully developed state. In the entrance region, variation of velocity near the wall along vertical direction is large.

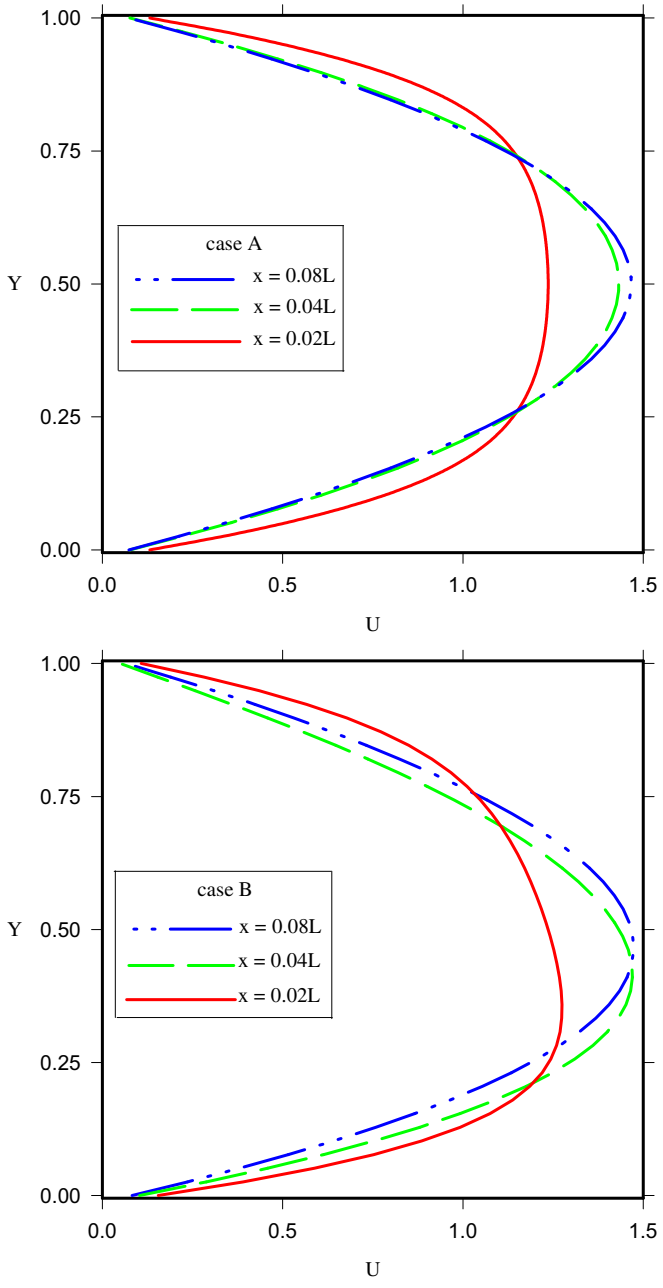

Fig. 7. Profiles of U in different cross sections at Kn = 0.01 for the cases A and B.

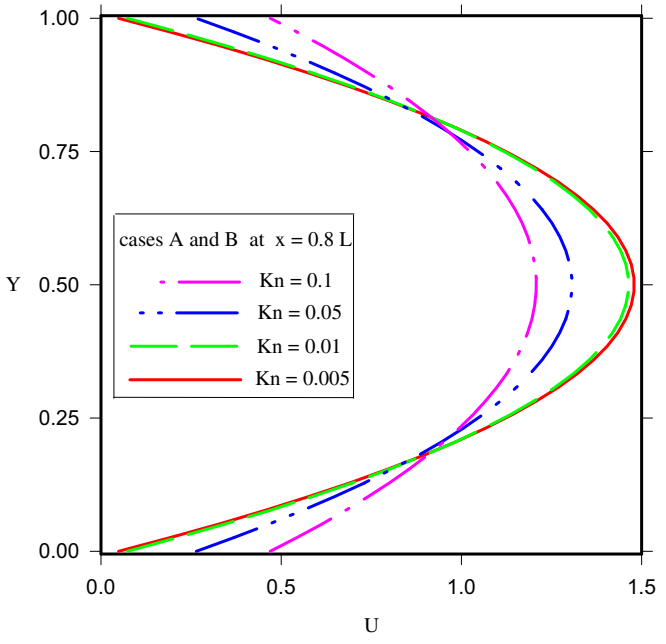

Fig. 8. Profiles of U in the cross section, $x = 0.8L$, for different Kn's for the cases A and B.

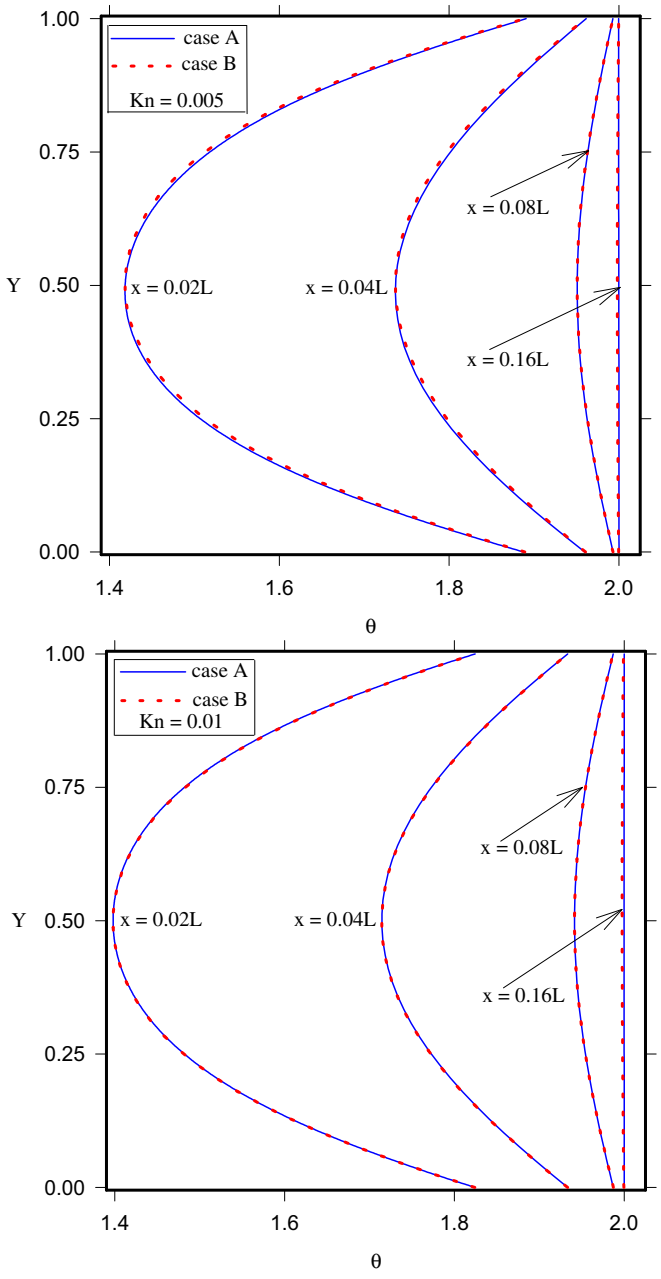

Fig. 9. Profiles of θ in different cross sections at Kn = 0.005, 0.01 for the cases A and B.

The velocity along the microchannel approaches its maximum on the horizontal centerline; however, the slip velocity continues decreasing after reaching the fully developed condition, and then approaches a constant value.

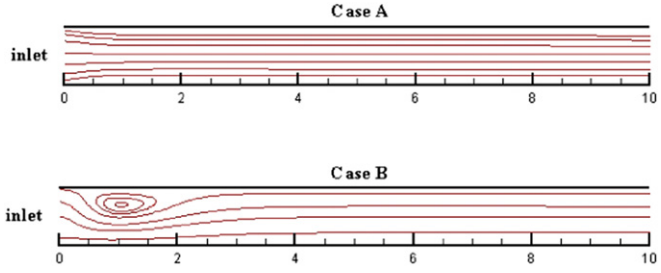

Fig. 10. Streamlines at Kn = 0.005 for the cases A and B.

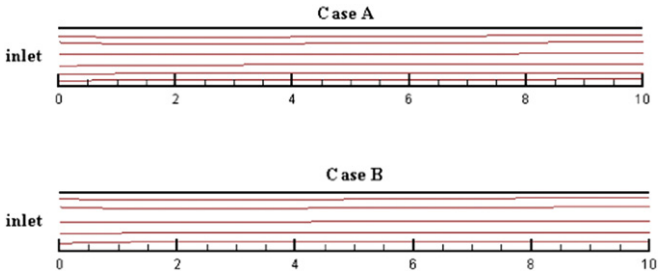

Fig. 11. Streamlines at Kn = 0.1 for the cases A and B.

In the case B, the variation of velocity profiles in the entrance region increases. In addition, a back flow in the top half of the microchannel occurs at $Y > 0.6$ and $x = 0.04$L. This backflow makes a counterclockwise rotational cell, which shows the importance of buoyancy forces in this regime. The buoyancy forces decreases with x, making gradually the velocity profile symmetrical. The high temperature difference between the fluid and walls, in the entrance region, generates powerful buoyancy forces. Fig. 6 illustrates the negative slip velocity for the case B, on the top wall ($Y = 1$) due to the backflow of the rotational cell. This new physical phenomenon, resulting from gravity effects, has not been observed in previous works.

Fig. 7 shows that velocity profiles in the cases A and B become more similar at Kn = 0.01. Case B of this figure shows that fluid flow is pushed downward because of gravity effects in the entrance region, thus U_{max} at $x = 0.02$L occurs at around $Y = 0.25$. Figs. 6 and 7 show a higher value of Kn corresponds to a higher slip velocity (U_s). More studies show that as Kn increases, the corresponding velocity profiles for these cases approaches each other and at last approximately coincide.

Fig. 8 shows profile of horizontal component of velocity, U, for the cases A and B in the cross section far from the inlet, $x = 0.8$ L, for different values of Kn. It is observed that there is a slight difference between the profiles of cases A and B. So, the effects of gravity in the entrance region are more significant than fully developed region.

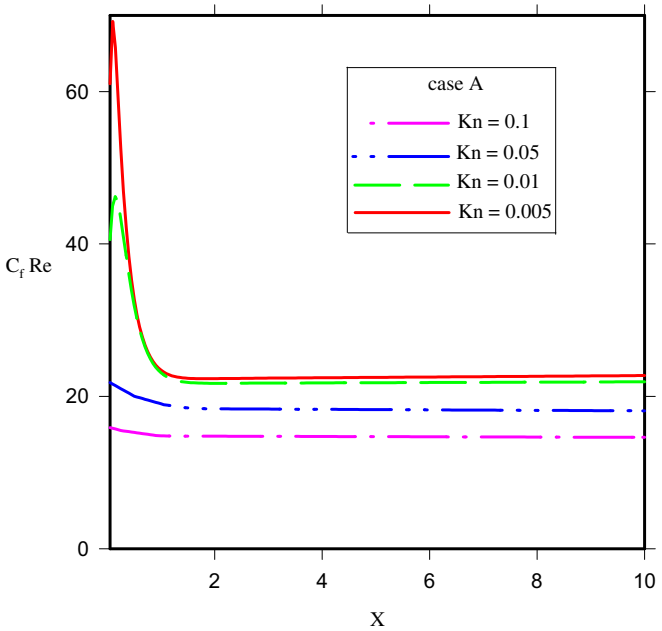

Fig. 12. Variations of C_fRe along the microchannel walls for the case A at different Kn's.

Fig. 9 shows profiles of dimensionless temperature, $\theta = T/T_{in}$, in different cross sections, for the cases A and B, at Kn = 0.005 and Kn = 0.01, respectively.

It is observed that the fluid temperature increases because of heat exchange with hot walls. The fluid temperature at $x = 0.16L$ approaches the walls temperature. After this point, there will be no significant mixed convection heat transfer, and the fluid flow will be completely isothermal. This flow behavior results form the strong effects of buoyancy forces in the entrance region. Comparison between the plots for Kn = 0.005 and Kn = 0.01 in this figure shows a higher value of Kn corresponds to a higher temperature jump. In addition, it is observed that the temperature profiles of the cases A and B become more similar at larger Kn, so that they coincide at Kn = 0.05 and Kn = 0.1.

Figs. 10 and 11 show streamlines at Kn = 0.005 and 0.1 for the cases A and B respectively. In Fig. 10 (case A) flow enters the microchannel from the left side and leaves it from the right side. In this mode, streamlines are completely symmetric along the horizontal central line of microchannel, and the variations in the fluid flow properties are seen only in the little space of the entrance region. Case B in this figure shows clearly the effect of gravity acceleration in generating buoyancy motions in the entrance length. After flow entering the microchannel, its streamlines move downward due to the effect of gravity and then move upward because of being heated. This causes the rotational cell to be generated in this area, as it was explained before. Fig. 11 shows that with the increase of Kn, the strength of the cell is reduced, so that at Kn = 0.1, streamlines become parallel, without any rotational cell, and independent of buoyancy motions.

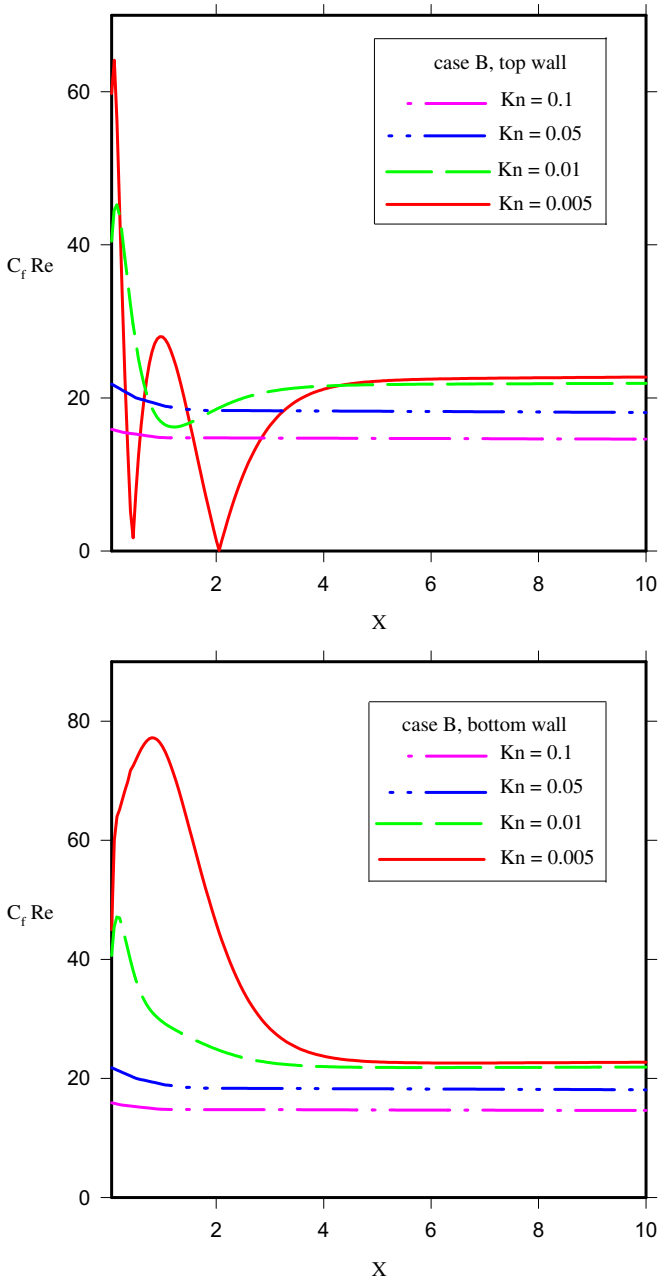

Fig. 13. Variations of C_fRe along the top and bottom walls for the case B at different Kn's.

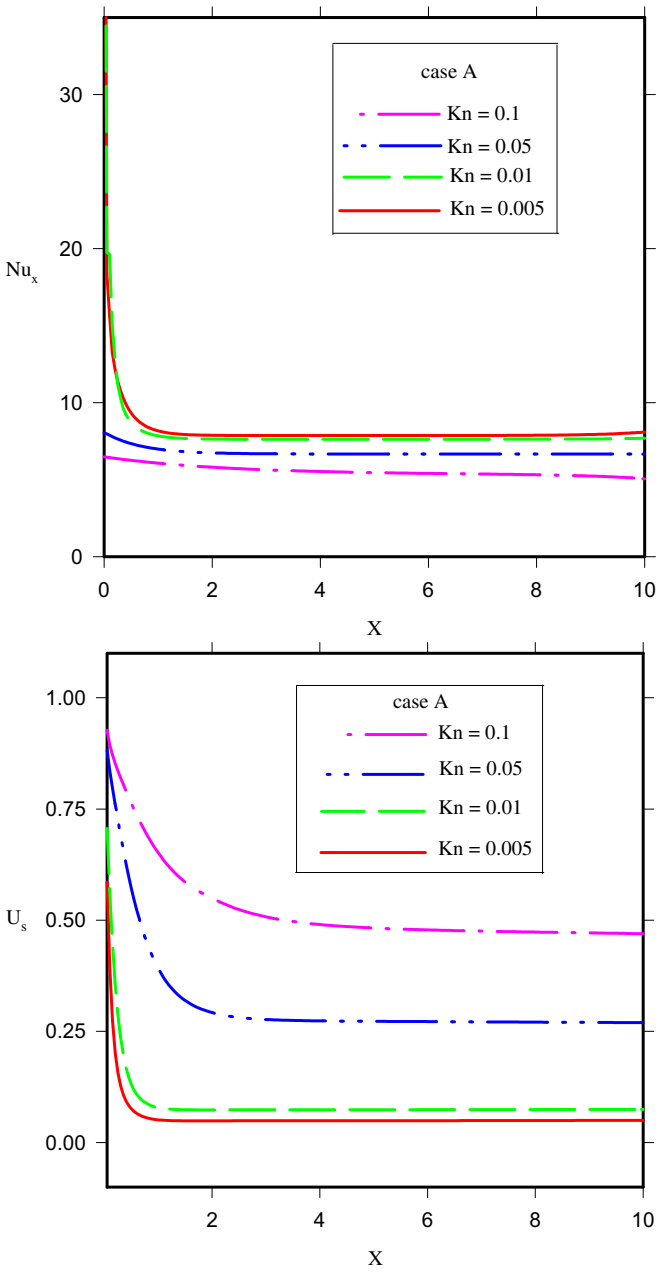

Fig. 14. Variations of *Nu* and U_s along the walls of the microchannel at different Kn's for the case A.

Figs. 12 and 13 show variation of C_fRe along the walls of the microchannel for the cases A and B, for different Kn's. Fig. 12 shows for Kn = 0.005, C_fRe has larger value and starts from its maximum at the inlet and decreases asymptotically along the microchannel and approaches a constant value at the outlet. It is observed that slip velocity increases with Kn, meaning that the velocity gradients between the fluid particles on the wall and their neighbors, and as a result the value of C_f, will decrease.

Fig. 13 shows the value of C_fRe for the top and bottom walls are different at Kn = 0.005 and Kn = 0.01. Its large variations on the top wall for Kn = 0.005 is related to the beginning and end points of the rotational cell. The related results for the cases A and B on the top and bottom walls approach each other at larger values of Kn as 0.05 and 0.1.

Fig. 14 shows variation of *Nu* and slip velocity, U_s, along the walls of the microchannel at different Kn's for the case A. It is observed that *Nu* and U_s start from their maximum at the inlet and decreases asymptotically along the microchannel and approaches a constant value at the outlet. Also, it is observed that the increase of Kn leads to the decrease of *Nu* and increase of U_s. It is observed that at larger Kn's, temperature gradient between the fluid particles on the wall and their neighbors, and as a result *Nu*, decreases.

Moreover, in the case B the buoyancy force, does not have significant effect on *Nu* and the results will be very similar to those of Fig. 14.

Fig. 15 shows variation of slip velocity, U_s, along the walls of the microchannel at different Kn's for the case B, respectively. It is seen the variations of U_s along the top and bottom walls are the same for

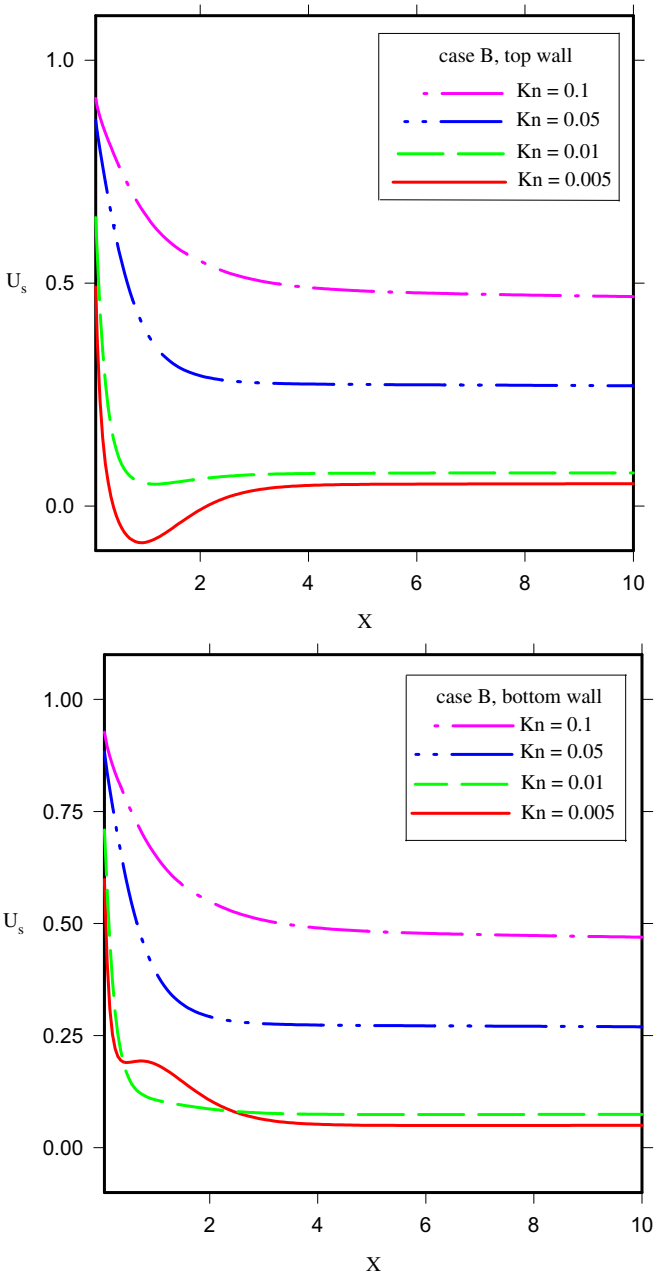

Fig. 15. Variations of U_s along the top and bottom walls of the microchannel at different Kn's for the case B.

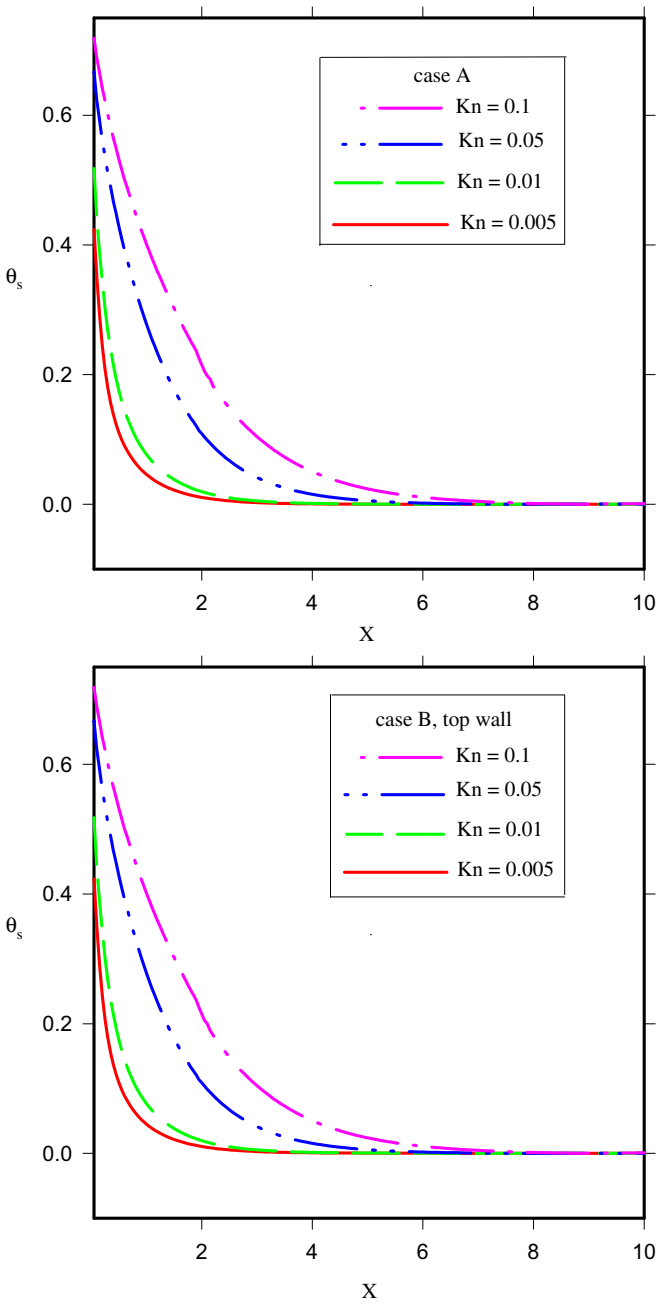

Fig. 16. Variations of temperature jump, θ_s, along the top wall of the microchannel at different Kn's for the cases A and B.

Kn = 0.05, 0.1. But at smaller Kn's,gravity effects are increased, leading to the increase of the difference between the results. For Kn = 0.005 the slip velocity profiles along the top and bottom walls are completely different with each other and with the corresponding values in the case A. However, at the distance far from the entrance region the results of Figs. 15 and 14 becomes similar. In addition, the negative slip velocity is observed on the top wall of the microchannel at Kn = 0.005 for $x < 2$, confirming the existence of the counterclockwise cell in this region.

Fig. 16 shows the variation of temperature jump, θ_s, along the top wall of the microchannel at different Kn's for the cases A and B, respectively. It is observed that temperature jump increases with inlet Kn; however, it decreases along the microchanel.

6. Conclusion

The effects of gravity on the flow and mixed convection heat transfer inside a two-dimensional microchannel for a wide range of Kn were investigated using LBM-BGK. To include the effect of gravity, in addition to the force convection flow, the hydrodynamic boundary condition equations were modified.

It was observed that with the increase of Kn, the slip velocity and temperature jump are increased, and Nu and C_f are reduced. The maximum value of theses parameters occurs at the inlet, and they approach asymptotically to the corresponding constant value along the microchannel.

The effects of gravity generate buoyancy motions, particularly in the entrance region that has the largest temperature gradient between the fluid and the walls, and thus increase the entrance length. Mixed convection motions cause large variations in the hydrodynamics of flow such as the slip velocity and friction coefficient and generate a counterclockwise cell. The negative slip velocity, which was revealed for the first time in this work, results from this cell and covers almost large fraction of the entrance region.

Increase of Kn led to decrease the buoyancy motions and dominant mechanism of heat transfer tended to forced convection. Lattice Boltzmann method with proposed modifications, could be used to simulate the effects of gravity and mixed convection in a microchannel flow and heat transfer. It is recommended that for Kn < 0.05 the effects of gravity are important, specially for hydrodynamic properties, and should be included. For Kn > 0.05, these effects can be ignored.

References

[1] N.T. Nguyen, S.T. Wereley, Fundamentals and Applications of Microfluidics, second ed. Artech house INC, Norwood, MA 02062, 2006.
[2] M. Gad-el-Hak, Flow physics in MEMS, Rev. Mec. Ind. 2 (2001) 313–341.
[3] T.M. Adams, S.I. Abdel-Khalik, S.M. Jeter, Z. Quresi, An experimental investigation of single-phase forced convection in microchannels, Int. J. Heat Mass Transfer 41 (1998) 851–857.
[4] Y. Xuan, Q. Li, M. Ye, Investigations of convective heat transfer in ferrofluid microflows using lattice-Boltzmann approach, Int. J. Thermal Sci. 46 (2007) 105–111.
[5] X. Nie, G.D. Doolen, S. Chen, Lattice-Boltzmann simulation of fluid flows in MEMS, J. Stat. Phys. 107 (2002) 279–289.
[6] C. Ho, Y. Tai, Micro-electro-mechanical-systems (MEMS) and fluid flows, Annu. Rev. Fluid Mech. 30 (1998) 579–612.
[7] G. Bird, Molecular Gas Dynamics and the Direct Simulation of Gas Flows, Oxford University Press, 1994.
[8] E.S. Oran, C.K. Oh, B.Z. Cybyk, Direct simulation Mont Carlo: recent advances and applications, Ann. Rev. Fluid Mech. 30 (1998) 403–441.
[9] S. Kandlikar, S. Garimella, D. Li, S. Colin, M.R. King, Heat Transfer and Fluid Flow in Minichannels and Microchannels (2006).
[10] S. Chen, G.D. Doolen, Lattice Boltzmann method for fluid flows, Annu. Rev. Fluid Mech. 30 (1998) 329–364.
[11] C. Chang, Y.T. Yang, T.H. Yen, C.K. Chen, Numerical investigation into thermal mixing efficiency in Y-shaped channel using Lattice Boltzmann method and field synergy principle, Int. J. Thermal Sci. 48 (2009) 2092–2099.
[12] M. Wang, J. He, J. Yu, N. Pan, Lattice Boltzmann modeling of the effective thermal conductivity for fibrous materials Int, J. Thermal Sci. 46 (2007) 848–855.
[13] H.P. Kavehpour, M. Faghri, Y. Asako, Effects of compressibility and rarefaction on gaseous flows in microchannels, Numer. Heat Transfer, Part A 32 (1997) 677–696.
[14] W.A. Zahid, Y. Yin, K. Zhu, Couette-Poiseuille flow of a gas in long microchannels, Microfluid Nanofluid 3 (2007) 55–64.
[15] S. Succi, The Lattice Boltzmann Equation for Fluid Dynamics and Beyond, Oxford University Press, Oxford, 2001.
[16] K. Han, Y.T. Feng, D.R.J. Owen, Modelling of thermal contact resistance within the framework of the thermal lattice Boltzmann method, Int. J. Thermal Sci. 47 (2008) 1276–1283.
[17] S. Chen, Z. Tian, Entropy generation analysis of thermal micro-Couette flows in slip regime, Int. J. Thermal Sci. 49 (2010) 2211–2221.
[18] A. Al-Zoubi, G. Brenner, Simulating fluid flow over sinusoidal surfaces using the lattice Boltzmann method, Comput. Math. Appl. 55 (2008) 1365–1376.
[19] P.L. Bhatnagar, E.P. Gross, M. Krook, A model for collision process in gases. I. Small amplitude processes in charged and neutral one-component system, Phys. Rev. 94 (1954) 511–522.
[20] X. He, S. Chen, G.D. Doolen, A novel thermal model for the lattice Boltzmann method in incompressible limit, J. Computational Phys. 146 (1998) 282–300.
[21] Z. Guo, B. Shi, N. Wang, Lattice BGK model for incompressible Navier–Stokes equation, J. Computational Phys. 165 (2000) 288–306.
[22] A. D'Orazio, M. Corcione, G.P. Celata, Application to natural convection enclosed flows of a lattice Boltzmann BGK model coupled with a general purpose thermal boundary condition, Int. J. Thermal Sci. 43 (2004) 575–586.
[23] A. D'Orazio, S. Succi, Simulating two-dimensional thermal channel flows by means of a lattice Boltzmann method with new boundary conditions, Future Generation Comput. Syst. 20 (2004) 935–944.
[24] A. D'Orazio, S. Succi, C. Arrighetti, Lattice Boltzmann simulation of open flows with heat transfer, Phys. Fluids 15 (2003) 2778–2781.
[25] Y. Zhou, R. Zhang, I. Staroselsky, H. Chen, W.T. Kim, M.S. Jhon, Simulation of micro- and nano-scale flows via the lattice Boltzmann method, Physica 362 (2006) 68–77.
[26] S. Chen, Lattice Boltzmann method for slip flow heat transfer in circular microtubes: extended Graetz problem, Appl. Math. Comput. 217 (2010) 3314–3320.
[27] C.Y. Lim, C. Shu, X.D. Niu, Y.T. Chew, Application of lattice Boltzmann method to simulate microchannel flows, Phys. Fluids 14 (2002) 2299–2308.
[28] X.D. Niu, C. Shu, Y.T. Chew, A thermal lattice Boltzmann model with diffuse scattering boundary condition for micro thermal flows, Comput. Fluids 36 (2007) 273–281.
[29] X.D. Niu, C. Shu, Y.T. Chew, A lattice Boltzmann BGK model for simulation of micro flows, Europhys. Lett. 67 (4) (2004) 600–606.
[30] C. Shu, X.D. Niu, Y.T. Chew, A lattice Boltzmann kinetic model for microflow and heat transfer, J. Stat. Phys. 121 (2005) 239–255.
[31] V. Sofonea, R.F. Sekerka, Boundary conditions for the upwind finite difference Lattice Boltzmann model: evidence of slip velocity in micro-channel flow, J. Computational Phys. 207 (2005) 639–659.
[32] Y.H. Zhang, R.S. Qin, Y.H. Sun, R.W. Barber, D.R. Emerson, Gas flow in microchannels - A lattice Boltzmann method approach, J. Stat. Phys. 121 (2005) 257–267.
[33] W.C. Hung, Y. Ru, A numerical study for slip flow heat transfer, Appl. Math. Comput. 173 (2006) 1246–1264.
[34] Z.W. Tian, C. Zou, H.J. Liu, Z.L. Guo, Z.H. Liu, C.G. Zheng, Lattice Boltzmann scheme for simulating thermal micro-flow, Physica 385 (2007) 59–68.
[35] L. Szalmas, Multiple-relaxation time lattice Boltzmann method for the finite Knudsen number region, Physica 379 (2007) 401–408.
[36] S.H. Kim, H. Pitsch, I.D. Boyd, Accuracy of higher-order lattice Boltzmann methods for microscale flows with finite Knudsen numbers, J. Computational Phys. 227 (2008) 8655–8671.
[37] F. Verhaeghe, L.S. Luo, B. Blanpain, Lattice Boltzmann modeling of microchannel flow in slip flow regime, J. Computational Phys. 228 (2009) 147–157.
[38] H. Babovsky, A numerical model for the Boltzmann equation with applications to micro flows, Comput. Math. Appl. 58 (2009) 791–804.
[39] S. Chen, Z. Tian, Simulation of microchannel flow using the lattice Boltzmann method, Physica 388 (2009) 4803–4810.
[40] S. Chen, Z. Tian, Simulation of thermal micro-flow using lattice Boltzmann method with Langmuir slip model, Int. J. Heat Fluid Flow 31 (2010) 227–235.
[41] Z. Tian, S. Chen, C.G. Zheng, Lattice Boltzmann simulation of gaseous finite-Kundsen microflows, Int. J. Mod. Phys. C 21 (2010) 769–783.
[42] Y.H. Qian, D. d'Humieres, P. Lallemand, Lattice BGK models for Navier-Stokes equation, Europhys. Lett. 17 (1992) 479–484.
[43] Q. Zou, X. He, On pressure and velocity boundary conditions for the lattice Boltzmann BGK model, Phys. Fluids 9 (1997) 1591–1599.
[44] A.A. Alamyane, A.A. Mohamad, Simulation of forced convection in a channel with extended surfaces by the lattice Boltzmann method, Comput. Math. Appl. 59 (2010) 2421–2430.
[45] G. Karniadakis, A. Beskok, Micro Flows: Fundamentals and Simulation, Springer, New York, 2002.
[46] S. Succi, Mesoscopic modelling of slip motion at fluid-solid interfaces with heterogeneous catalysis, Phys. Rev. Lett. 89 (2002) 064502.
[47] G.V. Davis, Natural convection of air in a square cavity: a benchmark numerical solution, Int. J. Numer. Methods Fluids 3 (1983) 249–264.
[48] S. Habchi, S. Acharya, Laminar mixed convection in a partially blocked, vertical channel, Int. J. Heat Mass Transfer 29 (1986) 1711–1722.